

Gapless Criterion for Crystals from Effective Axion Field

Jiabin Yu,^{1,*} Zhi-Da Song,² and Chao-Xing Liu¹

¹*Department of Physics, the Pennsylvania State University, University Park, PA, 16802*

²*Department of Physics, Princeton University Princeton, NJ 08544, USA*

Gapless criteria that can efficiently determine whether a crystal is gapless or not are particularly useful for identifying topological semimetals. In this work, we propose a sufficient gapless criterion for three-dimensional non-interacting crystals, based on the simplified expressions for the bulk average value of the static axion field. The brief logic is that two different simplified expressions give the same value in an insulator, and thus the gapless phase can be detected by the mismatch of them. We apply the gapless criterion to the magnetic systems with space groups 26 and 13, where mirror, glide, and inversion symmetries provide the simplified expressions, and find that it can be effective in systems with or without spin-orbit coupling. In particular, the gapless criterion can identify gapless phases that are missed by the symmetry-representation approach, as illustrated by space group 26. Our proposal serves as a guiding principle for future discovery of topological semimetals.

I. INTRODUCTION

Complementary to the study on topological insulators^{1,2}, the last decade has witnessed intense research interests in three dimensional (3D) topological semimetals^{3–18}. The search for material candidates is a central topic in this field. Recently, thousands of topological semimetals^{19–22} has been proposed based on the symmetry eigenvalue analysis^{23–29} (or more precisely counting symmetry representations at high-symmetry momenta). The high efficiency of the approach originates from the fact that it only requires the information of the ground state wavefunction in a lower dimensional submanifold of 3D first Brillouin zone (1BZ), like high-symmetry points/lines/planes. However, many gapless phases cannot be identified with the symmetry-representation approach, especially when the gapless points locate at generic momenta³⁰, such as the Weyl semimetal TaAs^{8–10}. Therefore, new efficient gapless criteria that can help fix this issue are of particular importance.

In this work, we exploit the effective axion field θ of 3D materials and propose an efficient gapless criterion that can detect gapless phases beyond the symmetry-representation approach. The dimensionless θ appears in the electromagnetic response of 3D insulating crystals as^{31,32}

$$\mathcal{L}_\theta = \frac{e^2}{hc} \frac{\theta}{2\pi} \mathbf{E} \cdot \mathbf{B}, \quad (1)$$

where e , h , and c are the elementary charge, Planck constant, and speed of light, respectively. Based on symmetries, several simplified expressions^{23,24,33–36} have been derived for evaluating the average value of static θ in the bulk of materials. The key idea of this work is to check the consistency of these simplified expressions. Intuitively, when two expressions mismatch, it means θ is not well-defined, indicating the possible existence of gapless points. The gapless criterion is efficient since the simplified expressions only involve lower dimensional submanifolds of 1BZ. We demonstrate the effectiveness of this gapless criterion in two magnetic systems: one with

space group (SG) 26 and spin-orbit coupling (SOC), and the other with SG 13 but without SOC. In the first example, we find that the gapless criterion can identify Weyl semimetal phases beyond the symmetry-representation approach, while the gapless criterion agrees with the symmetry-representation approach in the second example.

II. EFFECTIVE AXION FIELD

Before discussing the gapless criterion, we review the static effective axion field in 3D crystals and the simplified expressions given by symmetries. We focus on insulators with vanishing quantum anomalous Hall (QAH) conductivity (or equivalently with zero Chern number (CN) on any 2D plane parallel to any two of the three primitive reciprocal lattice vectors), like time-reversal (TR) invariant insulators^{31,33}. In these insulators, the bulk average value of the static effective axion field can be expressed as^{31–33}

$$\theta = \frac{1}{4\pi} \int d^3k \epsilon^{ijl} \text{Tr}[A_i \partial_{k_j} A_l + i \frac{2}{3} A_i A_j A_l], \quad (2)$$

where θ labels the bulk average value henceforth, duplicated indexes are summed over, and $[A_i(\mathbf{k})]_{a_1 a_2} = -i \langle u_{\mathbf{k}, a_1} | \partial_{k_i} | u_{\mathbf{k}, a_2} \rangle$ is the Berry connection. $|u_{\mathbf{k}, a}\rangle$'s are the cell-periodic parts of the occupied Bloch states, and are required to be globally continuous^{23,33,35} in the above expression. As a result of this gauge choice, the index $a = 1, \dots, N$ with N the number of occupied bands may not be the band index. The existence of such globally continuous gauge for the occupied subspace is guaranteed by the zero CNs³⁷. To keep the global continuity of the gauge, the $U(N)$ gauge transformation, $|u_{\mathbf{k}, a}\rangle \rightarrow |u_{\mathbf{k}, a'}\rangle [U(\mathbf{k})]_{a' a}$, allowed in Eq. (2) must also be continuous everywhere. Such gauge transformations can only change θ by multiplicities of 2π , making θ unambiguous modulo 2π . Eq. (2) is hard to use in general, since we need to know the occupied Bloch wavefunctions in the entire 1BZ and derive the globally continuous bases from them.

In the presence of a so-called “axion-odd” symmetry^{23,24,31–36,38–42}, $\theta \bmod 2\pi$ is quantized to 0 or π . The axion-odd symmetry is either an improper SG symmetry or a combination of TR symmetry and a proper SG symmetry, where “proper” and “improper” mean that the point group part of the SG operation has determinant 1 and -1 , respectively, when acting on the real space position. In appropriate setups, physical consequences of $\theta = \pi$ include quantized magnetoelectric effect^{31,43}, quantized zero Hall plateau^{44–46}, Faraday and Kerr rotation^{47–49}. Recently, such symmetry-protected $\theta = \pi$ phase has been predicted to exist in magnetic materials $(\text{MnTe})_n(\text{Bi}_2\text{Te}_3)_m$ ^{50,51}.

The complicated task of evaluating θ can be simplified by certain axion-odd symmetries, which we call “axion-odd-simplification” (AOS) symmetries. An axion-odd symmetry g is an AOS symmetry if it can provide a simplified expression ν_g for θ such that ν_g is only defined on a lower-dimensional submanifold of 1BZ and is gauge-invariant. The gauge-invariance means we can evaluate ν_g without explicitly finding the globally continuous gauge. A widely known AOS symmetry is the inversion symmetry^{23,24}, whose simplified expression ν_P for θ reads

$$\frac{\theta}{\pi} \bmod 2 = \nu_P = \frac{\kappa_4}{2}, \quad (3)$$

where

$$\kappa_4 = \sum_{\mathbf{K}} \frac{n_{\mathbf{K}}^{P,+} - n_{\mathbf{K}}^{P,-}}{2} \bmod 4, \quad (4)$$

$n_{\mathbf{K}}^{P,\pm}$ labels the number of occupied states with inversion eigenvalue ± 1 at the inversion-invariant momentum \mathbf{K} , and the sum of \mathbf{K} ranges over all inversion-invariant momenta as shown in Fig. 1(a). κ_4 can only be 0 or 2 in insulators, meaning that ν_P is a Z_2 index for insulators.

Mirror is also an AOS symmetry. Without loss of generality, we consider the mirror operation m_x that flips x . On a mirror-invariant plane ($k_x = \Lambda$ with $\Lambda = 0, \pi$ as shown in Fig. 1(b)), the occupied states have definite mirror eigenvalues $\pm s$, where $s = 1$ without SOC and $s = i$ with SOC. A related topological invariant, called “mirror CN”⁵², can then be defined as

$$C_{k_x=\Lambda}^M = \frac{C_{k_x=\Lambda}^{m_x,+} - C_{k_x=\Lambda}^{m_x,-}}{2}, \quad (5)$$

where $C_{k_x=\Lambda}^{m_x,\pm}$ is the total CN of occupied bands with mirror eigenvalue $\pm s$. Finally, the simplified expression for θ given by mirror, labeled as ν_{m_x} , reads^{34,42}

$$\frac{\theta}{\pi} \bmod 2 = \nu_{m_x} = C_{k_x=0}^M - C_{k_x=\pi}^M \bmod 2. \quad (6)$$

Similar situation happens for the glide symmetry. Without loss of generality, we consider the glide symmetry $g_y = \{m_y | 00\frac{1}{2}\}$ that is the combination of half lattice translation along z and the mirror operation m_y

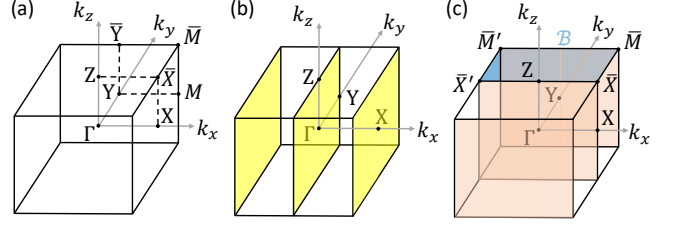


FIG 1. (a), (b) and (c) show the 1BZs for the inversion P , mirror m_x and glide g_y cases, respectively. Without loss of generality, we choose three primitive reciprocal lattice vectors to be orthogonal, and we, throughout the work, set the magnitudes of all primitive lattice vectors to be 1. In (a), the eight inequivalent inversion invariant points are marked by the black dots. The yellow planes in (b) are at $k_x = -\pi, 0, \pi$ and invariant under the mirror operation. In (c), the glide-invariant planes at $k_y = -\pi, 0, \pi$ are marked pink, and the blue area, labeled by \mathcal{B} , is parametrized as $k_x \in (-\pi, \pi]$, $k_y \in [0, \pi]$ and $k_z = \pi$.

that flips y . The states with $k_y = \Lambda$ can have definite glide eigenvalues $\pm s e^{-ik_z/2}$. Then, the simplified expression ν_{g_y} for θ reads^{42,44,53–55}

$$\frac{\theta}{\pi} \bmod 2 = \nu_{g_y} = C_{k_y=0}^{g_y,-} - C_{k_y=\pi}^{g_y,-} + C_{\mathcal{B}} - 2(\gamma_{\bar{X}'\bar{X}}^{g_y,-} + \gamma_{\bar{M}\bar{M}'}^{g_y,-}) \bmod 2. \quad (7)$$

$C_{k_y=\Lambda}^{g_y,-}$ and $C_{\mathcal{B}}$ are integrals of Berry curvature divided by 2π for the occupied bands with glide eigenvalue $-s e^{-ik_z/2}$ on plane $k_y = \Lambda$ and for all occupied bands in the area \mathcal{B} , respectively. (See Fig. 1(c) for details.) $\gamma_{\bar{X}'\bar{X}/\bar{M}\bar{M}'}^{g_y,-}$ labels the Berry phase divided by 2π for the occupied bands with glide eigenvalue $-s e^{-ik_z/2}$ along path $\bar{X}'\bar{X}/\bar{M}\bar{M}'$.

Other known AOS symmetries include TR³³ and the combination of TR and n -fold ($n = 2, 4$) rotational symmetries^{35,36} in the presence of SOC. All the examples show that the submanifold, on which the simplified expression is defined, mostly consists of high-symmetry momenta. Up to now, it is still unclear whether all axion-odd symmetries are AOS symmetries.

III. GAPLESS CRITERION

The gapless criterion that we propose is for crystals with at least two AOS symmetries, labeled as g_1 and g_2 . If the crystal is gapped and has zero CNs, the two simplified expressions, ν_{g_1} and ν_{g_2} , given by g_1 and g_2 for θ must be well-defined and equal (both equal to $\theta/\pi \bmod 2$). The contrapositive of the above statement is that the crystal is either gapped with non-zero CNs or gapless if (i) at least one of the two simplified expressions is ill-defined, or (ii) both simplified expressions are well defined but mismatch ($\nu_{g_1} \neq \nu_{g_2}$). Therefore, if the condition of the contrapositive is satisfied, the system must

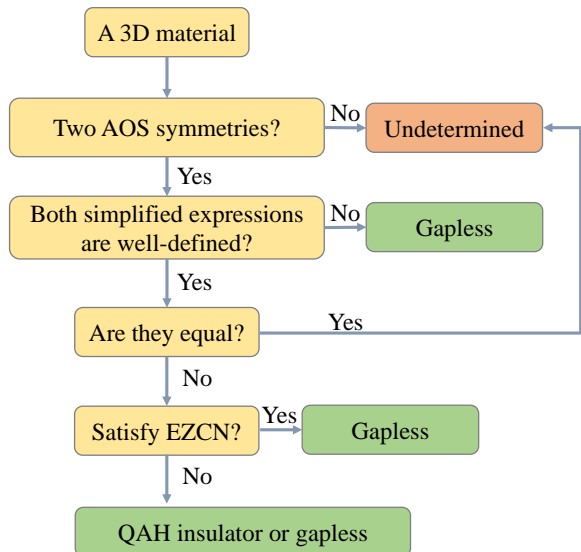


FIG 2. This flowchart demonstrates how to use the gapless criterion given a 3D material. Here “QAH insulator” means the system is gapped with nonzero CNs or equivalently non-vanishing QAH conductivity.

be in a non-trivial phase. In the case (i), the crystal must be gapless, since a simplified expression becomes ill-defined only if gapless points exist in the corresponding submanifold of 1BZ. However, the gapless points in this case are relatively simple to locate as the submanifold mostly consists of high symmetry momenta. So we focus on the case (ii) where gapless points stay away from the submanifolds.

In the case (ii), the possibility of insulators with non-zero CNs can be ruled out by the following “Existence-of-Zero-CN” (EZCN) condition: parallel to *any* two of the three primitive reciprocal lattice vectors, there *exist* a 2D plane in 1BZ on which the system is gapped and has zero CN. The EZCN condition is equivalent to zero CNs when the crystal is insulating, but it is satisfiable in gapless crystals. In particular, the EZCN condition can be naturally satisfied in the presence of certain symmetries, like SG 26 as discussed later, without imposing any other constraints. Fig. 2 summarizes the above logic in a flowchart, from which we derive a gapless criterion: given a crystal that has two AOS symmetries and satisfies the EZCN condition, it is gapless if the two simplified expressions are well-defined but mismatch. This is the main result of this work. In the following, we demonstrate the effectiveness of this gapless criterion for SG 26 and SG 13.

IV. MAGNETIC SYSTEMS WITH SG 26

We first study the spin-orbit coupled magnetic materials whose magnetic group is the same as SG 26 ($Pmc2_1$).

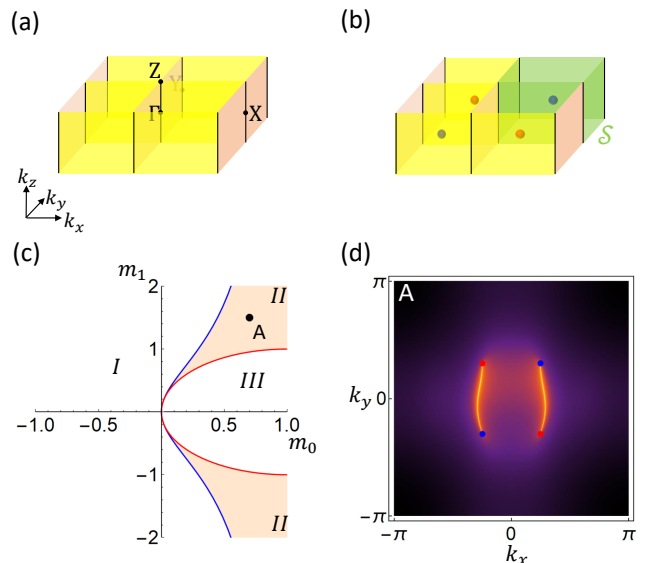


FIG 3. (a) shows the 1BZ of SG 26. The yellow and pink planes are invariant under m_x and g_y symmetries, respectively. The black lines are the intersections of those planes, where the little group is the entire SG. (b) demonstrates a distribution of Weyl points (red or blue dots) in a possible Weyl semimetal phase. The dots of the same (different) colors have the same (opposite) chiralities. The green area \mathcal{S} surrounds the $k_{x,y} > 0$ quarter of 1BZ. (c) is the phase diagram generated by the toy model. Phase I and III are insulating phases with $\theta = 0$ and $\theta = \pi$, respectively. Phase II is a Weyl semimetal phase that has the distribution of Weyl points as (b). The gap closes on $k_x = 0$ and $k_y = 0$ planes at the red and blue phase boundaries, respectively. (d) shows the Fermi arcs on (001) surface for point A in (c).

Besides lattice translations, SG 26 is generated by two AOS symmetries m_x and g_y . The primitive lattice vectors are orthogonal to each other (orthorhombic lattice). The inequivalent high symmetry momenta include two mirror-invariant planes ($k_x = 0, \pi$), two glide-invariant planes ($k_y = 0, \pi$), and their intersections, as shown in Fig. 3(a). We consider the case where the crystal is gapped at all these high-symmetry points. As a result, both ν_{m_x} and ν_{g_y} are well defined according to Eq. (6) and Eq. (7), since $C_{\mathcal{B}}$ is identically zero owing to m_x .

In the case that we consider, the symmetry representations furnished by the occupied bands at high-symmetry momenta are always the same as those of atomic insulators, according to Ref. [25 and 26]. However, the crystal can still be gapless, for example, having 4 Weyl points at generic momenta as shown in Fig. 3(b). Therefore, such gapless phase cannot be identified by the symmetry-representation approach. (see Appendix. A for more details.)

On the contrary, our gapless criterion is effective. Recall that the gapless criterion requires crystals to satisfy the EZCN condition. It turns out the condition is naturally satisfied here since m_x and g_y symmetries require the crystal to have zero CN on $k_x = 0$ plane, $k_y = 0$

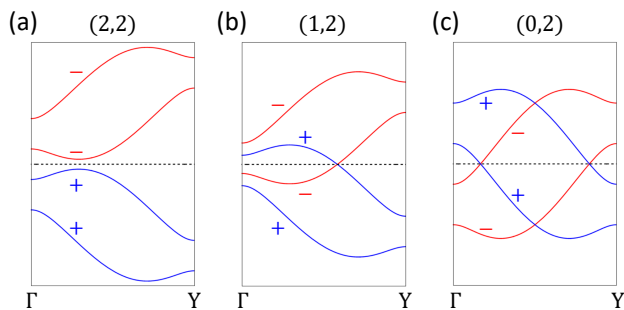


FIG 4. This figure includes schematic plots of band structures for SG 13 along $\Gamma - Y$. Blue and red lines are bands with R_2 eigenvalue $+1$ and -1 , respectively, and the black dotted line is the Fermi energy. The numbers in the brackets are values of $(n_{R_2,+}^\Gamma, n_{R_2,+}^Y)$, *i.e.*, the number of occupied states at Γ, Y with R_2 eigenvalue $+1$.

plane, and any plane perpendicular to z that does not contain any gapless points. Therefore, the gapless criterion is applicable for SG 26, indicating that the system is gapless when $\nu_{m_x} \neq \nu_{g_y}$. Further derivation (Appendix A) shows that, for the spin-orbit coupled case considered here, we have

$$\nu_{m_x} + \nu_{g_y} \pmod{2} = C_S \pmod{2}, \quad (8)$$

where C_S is the so-called ‘‘bend CN’’⁵⁶ over area S in Fig. 3(b). When $\nu_{m_x} \neq \nu_{g_y}$, C_S must be an odd number, and thus the corresponding gapless phase must contain an odd number of Weyl points in the quarter of 1BZ surrounded by S , *e.g.*, Fig. 3(b).

To verify the above analysis, we construct a toy model by putting a spinful s -orbital at the origin and symmetrizing it with SG 26. (See more details in Appendix A.) The resulting Hamiltonian is a four band model and has two tuning parameters m_0 and m_1 . We map out the phase diagram at half filling (2 occupied bands) in Fig. 3(c). There are two insulating phases, phase I with $(\nu_{m_x}, \nu_{g_y}) = (0, 0)$ and phase III with $(\nu_{m_x}, \nu_{g_y}) = (1, 1)$. As tuning the system from phase I to phase III, the gap closes on $k_y = 0$ plane at the blue boundary and ν_{g_y} changes from 0 to 1, resulting in phase II with $(\nu_{m_x}, \nu_{g_y}) = (0, 1)$. Phase II further evolves into phase III across the red boundary, where the gap closes on $k_x = 0$ plane and ν_{m_x} changes to 1. According to the gapless criterion and Eq. (8), phase II should be a WSM phase with odd C_S . Indeed, the phase contains 4 Weyl points symmetrically distributed on the $k_z = 0$ plane just like Fig. 3(b), and we plot the Fermi arcs on (001) surface in Fig. 3(d). The Fermi arcs are parts of the saddle-shape surface dispersion on (001) surface, as discussed in Appendix A.

V. MAGNETIC CRYSTALS WITH SG 13

In this section, we study the magnetic crystal whose magnetic group is SG 13 ($P2/c$) and whose SOC is neglectible. SG 13 contains two AOS symmetries, inversion P and glide g_y , and the primitive lattice vectors are orthogonal. Since the combined $R_2 = g_y P$ symmetry makes C_B identically zero, we choose the crystal to be gapped on the glide-invariant planes ($k_y = 0, \pi$) to keep ν_{g_y} and ν_P well-defined. (See Fig. 1(a,c).) To satisfy the EZCN condition, we further set the CN on $k_y = \pi$ to zero and keep the crystal gapped on $k_x = \pi$ and $k_z = \pi$ planes. The CNs on $k_x = \pi$ and $k_z = \pi$ planes naturally vanish owing to the glide symmetry.

With these conditions, the gapless criterion indicates the crystal is gapless if $\nu_P \neq \nu_{g_y}$. To understand its physical meaning, we first note that any state with $(k_x, k_z) = (0, 0)$ can have definite R_2 eigenvalues ± 1 . Then, by generalizing the result in Ref. [55], we obtain

$$\nu_P = \nu_{g_y} + \frac{n_{R_2,+}^\Gamma - n_{R_2,+}^Y}{2} \pmod{2}, \quad (9)$$

where $n_{R_2,+}^{\Gamma/Y}$ is the number of occupied states with R_2 eigenvalue $+1$ at Γ/Y . (See Appendix B for more details.) When the crystal is insulating, $n_{R_2,+}^\Gamma = n_{R_2,+}^Y$ must hold as exemplified in Fig. 4(a), consistent with $\nu_P = \nu_{g_y}$. When $\nu_P \neq \nu_{g_y}$, the nonzero $(n_{R_2,+}^\Gamma - n_{R_2,+}^Y)$ indicates the existence of R_2 -protected gapless points along $\Gamma - Y$ according to the symmetry-representation approach, as shown in Fig. 4(b-c). Therefore, the gapless criterion $\nu_P \neq \nu_{g_y}$ can identify the gapless phases detectable by the symmetry-representation approach.

VI. CONCLUSION AND DISCUSSION

Based on the effective axion field, we propose a gapless criterion for 3D crystals that have at least two AOS symmetries and satisfy the EZCN condition. The criterion is potentially applicable to systems with or without SOC and can identify gapless phases beyond the symmetry-representation approach. When applying this criterion in practice (say in first-principle calculations), it is better to follow Fig. 2 and check the EZCN condition at the very end, since the mismatch of two simplified expressions already indicates a non-trivial phase, QAH insulator or gapless. Our gapless criterion can serve as a guiding principle for the discovery of new topological semimetals.

As the gapless criterion can be more powerful if more AOS symmetries are identified, our proposal provides a driving force for future related theoretical study. Recently, Ref. [57] studied the spin-orbit coupled systems with TR and S_4 (four-fold rotation combined with inversion) symmetries, and demonstrated that some of its Weyl semimetal phases can be detected by the mismatch of two Z_2 indexes that are respectively protected by

the two symmetries. Therefore, it is intriguing to ask whether the Z_2 index of axion-odd S_4 is a simplified expression of θ . If so, the system serves as a TR-invariant example of our gapless criterion.

VII. ACKNOWLEDGEMENT

J.Y. thanks Biao Lian, Hoi Chun Po, and Xiao-Qi Sun for helpful discussions. Z.D.S. is supported by the

U.S. Department of Energy (grant no. DE-SC0016239), the National Science Foundation (EAGER grant no. DMR 1643312), Simons Investigator awards (grant no. 404513), ONR (grant no. N00014-14-1-0330), NSF-MRSEC (grant no. DMR-142051), the Packard Foundation, the Schmidt Fund for Innovative Research, and the Guggenheim Fellowship. J.Y. and C.X.L. acknowledge the support of the Office of Naval Research (Grant No. N00014-18-1-2793), the U.S. Department of Energy (Grant No. DESC0019064), and Kaufman New Initiative research grant KA2018-98553 of the Pittsburgh Foundation.

* jky5062@psu.edu

- ¹ M. Z. Hasan and C. L. Kane, *Rev. Mod. Phys.* **82**, 3045 (2010).
- ² X.-L. Qi and S.-C. Zhang, *Rev. Mod. Phys.* **83**, 1057 (2011).
- ³ A. A. Burkov, *Nature Materials* **15**, 1145 (2016).
- ⁴ B. Yan and C. Felser, *Annual Review of Condensed Matter Physics* **8**, 337 (2017).
- ⁵ A. Bernevig, H. Weng, Z. Fang, and X. Dai, *Journal of the Physical Society of Japan* **87**, 041001 (2018).
- ⁶ N. P. Armitage, E. J. Mele, and A. Vishwanath, *Rev. Mod. Phys.* **90**, 015001 (2018).
- ⁷ X. Wan, A. M. Turner, A. Vishwanath, and S. Y. Savrasov, *Phys. Rev. B* **83**, 205101 (2011).
- ⁸ H. Weng, C. Fang, Z. Fang, B. A. Bernevig, and X. Dai, *Phys. Rev. X* **5**, 011029 (2015).
- ⁹ S.-M. Huang, S.-Y. Xu, I. Belopolski, C.-C. Lee, G. Chang, B. Wang, N. Alidoust, G. Bian, M. Neupane, C. Zhang, S. Jia, A. Bansil, H. Lin, and M. Z. Hasan, *Nature Communications* **6**, 7373 (2015).
- ¹⁰ B. Q. Lv, H. M. Weng, B. B. Fu, X. P. Wang, H. Miao, J. Ma, P. Richard, X. C. Huang, L. X. Zhao, G. F. Chen, Z. Fang, X. Dai, T. Qian, and H. Ding, *Phys. Rev. X* **5**, 031013 (2015).
- ¹¹ A. A. Burkov, M. D. Hook, and L. Balents, *Phys. Rev. B* **84**, 235126 (2011).
- ¹² Z. Wang, Y. Sun, X.-Q. Chen, C. Franchini, G. Xu, H. Weng, X. Dai, and Z. Fang, *Phys. Rev. B* **85**, 195320 (2012).
- ¹³ Z. K. Liu, B. Zhou, Y. Zhang, Z. J. Wang, H. M. Weng, D. Prabhakaran, S.-K. Mo, Z. X. Shen, Z. Fang, X. Dai, Z. Hussain, and Y. L. Chen, *Science* **343**, 864 (2014).
- ¹⁴ A. A. Soluyanov, D. Gresch, Z. Wang, Q. Wu, M. Troyer, X. Dai, and B. A. Bernevig, *Nature* **527**, 495 (2015).
- ¹⁵ H. Weng, C. Fang, Z. Fang, and X. Dai, *Phys. Rev. B* **93**, 241202 (2016).
- ¹⁶ Z. Zhu, G. W. Winkler, Q. Wu, J. Li, and A. A. Soluyanov, *Phys. Rev. X* **6**, 031003 (2016).
- ¹⁷ T. Bzdusek, Q. Wu, A. Rüegg, M. Sigrist, and A. A. Soluyanov, *Nature* **538**, 75 (2016).
- ¹⁸ B. Bradlyn, J. Cano, Z. Wang, M. G. Vergniory, C. Felser, R. J. Cava, and B. A. Bernevig, *Science* **353** (2016), [10.1126/science.aaf5037](https://doi.org/10.1126/science.aaf5037).
- ¹⁹ M. G. Vergniory, L. Elcoro, C. Felser, N. Regnault, B. A. Bernevig, and Z. Wang, *Nature* **566**, 480 (2019).
- ²⁰ T. Zhang, Y. Jiang, Z. Song, H. Huang, Y. He, Z. Fang, H. Weng, and C. Fang, *Nature* **566**, 475 (2019).
- ²¹ F. Tang, H. C. Po, A. Vishwanath, and X. Wan, *Nature* **566**, 486 (2019).
- ²² B. Wieder, L. Elcoro, Z. Song, Y. Xu, N. Regnault, B. Bradlyn, and A. Bernevig, *Bulletin of the American Physical Society* (2020).
- ²³ A. M. Turner, Y. Zhang, R. S. K. Mong, and A. Vishwanath, *Phys. Rev. B* **85**, 165120 (2012).
- ²⁴ T. L. Hughes, E. Prodan, and B. A. Bernevig, *Phys. Rev. B* **83**, 245132 (2011).
- ²⁵ B. Bradlyn, L. Elcoro, J. Cano, M. Vergniory, Z. Wang, C. Felser, M. Aroyo, and B. A. Bernevig, *Nature* **547**, 298 (2017).
- ²⁶ H. C. Po, A. Vishwanath, and H. Watanabe, *Nature communications* **8**, 50 (2017).
- ²⁷ J. Kruthoff, J. de Boer, J. van Wezel, C. L. Kane, and R.-J. Slager, *Phys. Rev. X* **7**, 041069 (2017).
- ²⁸ Z. Song, T. Zhang, and C. Fang, *Phys. Rev. X* **8**, 031069 (2018).
- ²⁹ H. C. Po, [arXiv:2002.09391](https://arxiv.org/abs/2002.09391) (2020).
- ³⁰ Certain gapless points at generic momenta can be diagnosed through the symmetry-representation approach, like certain Weyl semimetal phases in the presence of inversion symmetry.
- ³¹ X.-L. Qi, T. L. Hughes, and S.-C. Zhang, *Phys. Rev. B* **78**, 195424 (2008).
- ³² A. M. Essin, J. E. Moore, and D. Vanderbilt, *Phys. Rev. Lett.* **102**, 146805 (2009).
- ³³ Z. Wang, X.-L. Qi, and S.-C. Zhang, *New Journal of Physics* **12**, 065007 (2010).
- ³⁴ D. Varjas, F. de Juan, and Y.-M. Lu, *Phys. Rev. B* **92**, 195116 (2015).
- ³⁵ J. Ahn and B.-J. Yang, *Phys. Rev. B* **99**, 235125 (2019).
- ³⁶ H. Li and K. Sun, *Phys. Rev. Lett.* **124**, 036401 (2020).
- ³⁷ C. Brouder, G. Panati, M. Calandra, C. Mourougane, and N. Marzari, *Phys. Rev. Lett.* **98**, 046402 (2007).
- ³⁸ C. Fang, M. J. Gilbert, and B. A. Bernevig, *Phys. Rev. B* **86**, 115112 (2012).
- ³⁹ N. Varnava and D. Vanderbilt, *Phys. Rev. B* **98**, 245117 (2018).
- ⁴⁰ F. Schindler, A. M. Cook, M. G. Vergniory, Z. Wang, S. S. P. Parkin, B. A. Bernevig, and T. Neupert, *Science Advances* **4** (2018), [10.1126/sciadv.aat0346](https://doi.org/10.1126/sciadv.aat0346).
- ⁴¹ B. J. Wieder and B. A. Bernevig, [arXiv:1810.02373](https://arxiv.org/abs/1810.02373) (2018).

- ⁴² N. Varnava, I. Souza, and D. Vanderbilt, [arXiv preprint arXiv:1912.11887](#) (2019).
- ⁴³ J. Yu, J. Zang, and C.-X. Liu, *Phys. Rev. B* **100**, 075303 (2019).
- ⁴⁴ J. Wang, B. Lian, X.-L. Qi, and S.-C. Zhang, *Phys. Rev. B* **92**, 081107 (2015).
- ⁴⁵ M. Mogi, M. Kawamura, A. Tsukazaki, R. Yoshimi, K. S. Takahashi, M. Kawasaki, and Y. Tokura, *Science Advances* **3** (2017), 10.1126/sciadv.aao1669.
- ⁴⁶ D. Xiao, J. Jiang, J.-H. Shin, W. Wang, F. Wang, Y.-F. Zhao, C. Liu, W. Wu, M. H. W. Chan, N. Samarth, and C.-Z. Chang, *Phys. Rev. Lett.* **120**, 056801 (2018).
- ⁴⁷ L. Wu, M. Salehi, N. Koirala, J. Moon, S. Oh, and N. Armitage, *Science* **354**, 1124 (2016).
- ⁴⁸ V. Dziom, A. Shuvaev, A. Pimenov, G. Astakhov, C. Ames, K. Bendias, J. Böttcher, G. Tkachov, E. Hankiewicz, C. Brüne, *et al.*, *Nature communications* **8**, 15197 (2017).
- ⁴⁹ K. N. Okada, Y. Takahashi, M. Mogi, R. Yoshimi, A. Tsukazaki, K. S. Takahashi, N. Ogawa, M. Kawasaki, and Y. Tokura, *Nature communications* **7**, 12245 (2016).
- ⁵⁰ D. Zhang, M. Shi, T. Zhu, D. Xing, H. Zhang, and J. Wang, *Phys. Rev. Lett.* **122**, 206401 (2019).
- ⁵¹ N. H. Jo, L.-L. Wang, R.-J. Slager, J. Yan, Y. Wu, K. Lee, B. Schunk, A. Vishwanath, and A. Kaminski, [arXiv:1910.14626](#) (2019).
- ⁵² J. C. Y. Teo, L. Fu, and C. L. Kane, *Phys. Rev. B* **78**, 045426 (2008).
- ⁵³ C. Fang and L. Fu, *Phys. Rev. B* **91**, 161105 (2015).
- ⁵⁴ K. Shiozaki, M. Sato, and K. Gomi, *Phys. Rev. B* **91**, 155120 (2015).
- ⁵⁵ H. Kim, K. Shiozaki, and S. Murakami, *Phys. Rev. B* **100**, 165202 (2019).
- ⁵⁶ A. Alexandradinata, C. Fang, M. J. Gilbert, and B. A. Bernevig, *Phys. Rev. Lett.* **113**, 116403 (2014).
- ⁵⁷ Y. Qian, J. Gao, Z. Song, S. Nie, Z. Wang, H. Weng, and Z. Fang, [arXiv preprint arXiv:1912.03961](#) (2019).
- ⁵⁸ L. Elcoro, B. Bradlyn, Z. Wang, M. G. Vergniory, J. Cano, C. Felser, B. A. Bernevig, D. Orobengoa, G. Flor, and M. I. Aroyo, *Journal of Applied Crystallography* **50**, 1457 (2017).
-

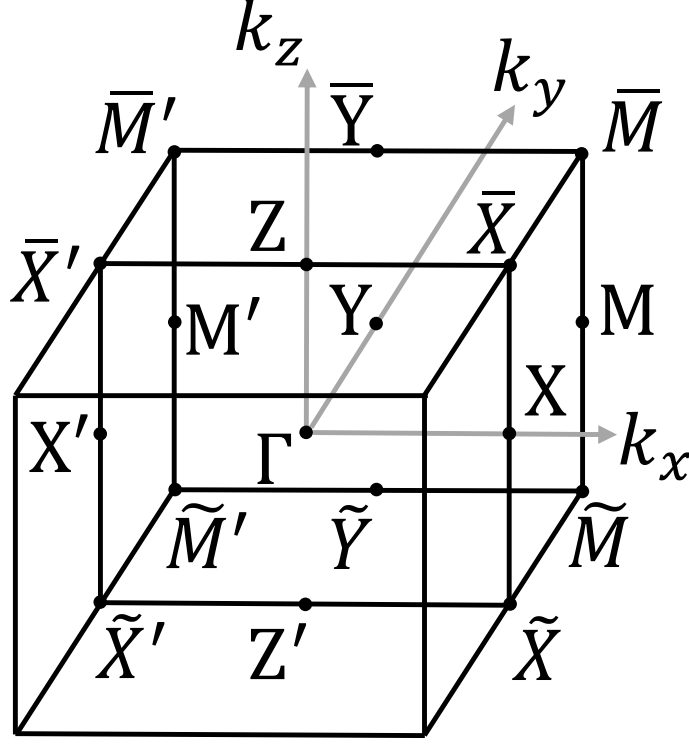


FIG 5. The 1BZ with more labels for SG 26 and SG 13.

Appendix A: More Details on SG 26 with SOC

In this section, we discuss SG 26 in more detail. We first discuss its symmetry representations at high-symmetry momenta, then derive Eq. (8) in the main text, and finally discuss the toy model. The high-symmetry points for this SG include the mirror invariant planes ($k_x = \Lambda$), the glide invariant planes ($k_y = \Lambda$), and their intersections, as shown in Fig. 3(a) of the main text. We always assume the system is gapped at all high-symmetry points. Useful points in 1BZ are labeled according to Fig. 5.

1. Symmetry Representations

In this part, we show that the symmetry representations at high symmetry points are the same as atomic insulators.

Owing to the existence of SOC, we have $m_x^2 = -1$, $g_y^2 = -\{\mathbb{1}|001\}$, and $\{m_x, g_y\} = 0$. Without loss of generality, we can always choose the Bloch states to be periodic along k_x and k_y , *i.e.*,

$$|\psi_{-\pi, k_y, k_z}\rangle = |\psi_{\pi, k_y, k_z}\rangle, \quad |\psi_{k_x, -\pi, k_z}\rangle = |\psi_{k_x, \pi, k_z}\rangle. \quad (\text{A1})$$

For $k_x = \Lambda$, the occupied Bloch states have definite mirror eigenvalue βi with $\beta = \pm$, labeled as $|\psi_{(\Lambda, k_y, k_z)}^{m_x, \beta, \alpha}\rangle$. Here $\alpha = 1, \dots, n_{(\Lambda, k_y, k_z)}^{m_x, \beta}$, and $n_{(\Lambda, k_y, k_z)}^{m_x, \beta}$ is the number of occupied states with mirror eigenvalue βi at (Λ, k_y, k_z) . Similarly, for $k_y = \Lambda$, the occupied Bloch states have definite glide eigenvalue $\beta i e^{-ik_z/2}$, labeled as $|\psi_{(k_x, \Lambda, k_z)}^{g_y, \beta, \alpha}\rangle$, where $\alpha = 1, \dots, n_{(k_x, \Lambda, k_z)}^{g_y, \beta}$, and $n_{(k_x, \Lambda, k_z)}^{g_y, \beta}$ is the number of occupied states with glide eigenvalue $\beta i e^{-ik_z/2}$ at (k_x, Λ, k_z) . Since the system is gapped at all high symmetry momenta, $n_{(\Lambda, k_y, k_z)}^{m_x, \beta}$ stay invariant as (k_y, k_z) changes, and so does $n_{(k_x, \Lambda, k_z)}^{g_y, \beta}$ as (k_x, k_z) varies. Therefore, we may relabel $n_{(\Lambda, k_y, k_z)}^{m_x, \beta}$ and $n_{(k_x, \Lambda, k_z)}^{g_y, \beta}$ as $n_{k_x=\Lambda}^{m_x, \beta}$ and $n_{k_y=\Lambda}^{g_y, \beta}$, respectively. Along k_z , $|\psi_{(\Lambda, k_y, k_z)}^{m_x, \beta, \alpha}\rangle$ can be chosen to be periodic

$$|\psi_{(\Lambda, k_y, -\pi)}^{m_x, \beta, \alpha}\rangle = |\psi_{(\Lambda, k_y, \pi)}^{m_x, \beta, \alpha}\rangle. \quad (\text{A2})$$

On the other hand, as $|\psi_{(k_x, \Lambda, \pm\pi)}^{g_y, \beta, \alpha}\rangle$ have opposite glide eigenvalues, we may choose

$$|\psi_{(k_x, \Lambda, -\pi)}^{g_y, \beta, \alpha}\rangle = |\psi_{(k_x, \Lambda, \pi)}^{g_y, -\beta, \alpha}\rangle, \quad (\text{A3})$$

which indicates $n_{k_y=\Lambda}^{g_y, -} = n_{k_y=\Lambda}^{g_y, +}$.

At the intersection of the mirror and glide planes $(k_x, k_y) = (\Lambda, \Lambda')$ with $\Lambda' = 0, \pi$, the Hamiltonian is invariant under both mirror and glide operations. $\{m_x, g_y\} = 0$ means that the irreducible representations (irreps) here are two-dimensional (2D), where m_x and g_y can be represented as⁵⁸

$$m_x \doteq -i \begin{pmatrix} 1 & \\ & -1 \end{pmatrix}, \quad g_y \doteq \begin{pmatrix} & -e^{-ik_z} \\ 1 & \end{pmatrix}. \quad (\text{A4})$$

We label such 2D irreps as Γ_2 , and label the number of Γ_2 irreps furnished by occupied states at $(k_x, k_y) = (\Lambda, \Lambda')$ as $n_{(\Lambda, \Lambda')}^{\Gamma_2}$, which is independent of k_z since the system is gapped at the intersection.

Now we include the rest of compatibility relations given by the fact that all high symmetry momenta are fully connected. First of all, the number of occupied bands should be the same at any high symmetry momentum, labeled as N . Then, one Γ_2 irrep at $(k_x, k_y) = (\Lambda, \Lambda')$ would split into two bands with opposite mirror (glide) eigenvalues as k_y (k_x) move away from the axis. Therefore, we have

$$\frac{N}{2} = n_{(0,0)}^{\Gamma_2} = n_{k_x=0}^{m_x, \pm} = n_{(0,\pi)}^{\Gamma_2} = n_{k_y=\pi}^{g_y, \pm} = n_{(\pi,\pi)}^{\Gamma_2} = n_{k_x=\pi}^{m_x, \pm} = n_{(\pi,0)}^{\Gamma_2} = n_{k_y=0}^{g_y, \pm}, \quad (\text{A5})$$

meaning that there are even number of the occupied bands, and $N/2$ is the only independent number.

If we put $N/2$ local orbitals with mirror eigenvalue $+i$ at the origin and symmetrize them with SG 26 (2a Wyckoff positions), we get the same symmetry representations as the above. Therefore, counting symmetry representations cannot identify any gapless phases in this case.

2. Derivation of Eq. (8) in the main text

In this part, we derive Eq. (8) in the main text. For convenience of the discussion, we use C to label the integral of Berry curvature divided by 2π for certain bands over certain region, γ to label the Berry phase divided by 2π for certain bands along certain path.

As described in the last part, the number N of occupied bands at high symmetry momenta is even, and we still adopt the same boundary condition, *i.e.*,

$$|\psi_{-\pi, k_y, k_z}^{m_x, \beta, \alpha}\rangle = |\psi_{\pi, k_y, k_z}^{m_x, \beta, \alpha}\rangle, \quad |\psi_{\Lambda, -\pi, k_z}^{m_x, \beta, \alpha}\rangle = |\psi_{\Lambda, -\pi, k_z}^{m_x, \beta, \alpha}\rangle, \quad |\psi_{\Lambda, k_y, -\pi}^{m_x, \beta, \alpha}\rangle = |\psi_{\Lambda, k_y, \pi}^{m_x, \beta, \alpha}\rangle, \quad (\text{A6})$$

$$|\psi_{-\pi, \Lambda, k_z}^{g_y, \beta, \alpha}\rangle = |\psi_{\pi, \Lambda, k_z}^{g_y, \beta, \alpha}\rangle, \quad |\psi_{k_x, -\pi, k_z}^{g_y, \beta, \alpha}\rangle = |\psi_{k_x, \pi, k_z}^{g_y, \beta, \alpha}\rangle, \quad |\psi_{k_x, \Lambda, -\pi}^{g_y, \beta, \alpha}\rangle = |\psi_{k_x, \Lambda, \pi}^{g_y, -\beta, \alpha}\rangle, \quad (\text{A7})$$

where $\alpha = 1, \dots, N/2$. The boundary conditions along k_x and k_y are natural, while the boundary condition for g_y eigenstates along k_z is special. Making such special choice along k_z does not influence the generality of the derivation since both Eq. (6) and Eq. (7) in the main text are gauge invariant and independent of the boundary conditions along k_z .

Owing to $\{m_x, g_y\} = 0$, we have

$$g_y |\psi_{\Lambda, k_y, k_z}^{m_x, \beta, \alpha}\rangle = |\psi_{\Lambda, -k_y, k_z}^{m_x, -\beta, \alpha'}\rangle V_{\alpha'\alpha}^{g_y, -\beta, \beta}(\Lambda, k_y, k_z), \quad m_x |\psi_{k_x, \Lambda, k_z}^{g_y, \beta, \alpha}\rangle = |\psi_{-k_x, \Lambda, k_z}^{g_y, -\beta, \alpha'}\rangle V_{\alpha'\alpha}^{m_x, -\beta, \beta}(k_x, \Lambda, k_z), \quad (\text{A8})$$

where those V matrices are unitary. Using the above relations and the fact that $C_{\mathcal{A}} - \gamma_{\partial\mathcal{A}} \in \mathbb{Z}$ with $\partial\mathcal{A}$ the boundary of \mathcal{A} , we can transform Eq. (6) and Eq. (7) in the main text to

$$\begin{aligned} \nu_{m_x} &= C_{ZZ'\tilde{Y}\tilde{Y}} - C_{\tilde{X}\tilde{X}\tilde{M}\tilde{M}} - 2\gamma_{ZZ'}^{m_x, +} - 2\gamma_{\tilde{Y}\tilde{Y}}^{m_x, +} + 2\gamma_{\tilde{X}\tilde{X}}^{m_x, +} + 2\gamma_{\tilde{M}\tilde{M}}^{m_x, +} \pmod{2}, \\ \nu_{g_y} &= C_{ZZ'\tilde{X}\tilde{X}} - C_{\tilde{M}\tilde{M}\tilde{Y}\tilde{Y}} - 2\gamma_{Z'\tilde{X}\tilde{X}Z'}^{g_y, +} - 2\gamma_{\tilde{M}\tilde{Y}\tilde{Y}\tilde{M}}^{g_y, +} - 2(\gamma_{\tilde{X}'\tilde{X}}^{g_y, -} + \gamma_{\tilde{M}\tilde{M}'}^{g_y, -}) \pmod{2}. \end{aligned} \quad (\text{A9})$$

Adding the two expression together yields

$$\begin{aligned} & \nu_{m_x} + \nu_{g_y} \pmod{2} \\ & = C_s - 2\gamma_{ZZ'}^+ - 2\gamma_{\bar{Y}\bar{Y}}^+ + 2\gamma_{\bar{X}\bar{X}}^+ + 2\gamma_{\bar{M}\bar{M}}^+ - 2\gamma_{Z\bar{X}}^{g_y,+} - 2\gamma_{\bar{X}'Z}^{g_y,-} + 2\gamma_{\bar{Y}\bar{M}}^{g_y,+} - 2\gamma_{\bar{Y}\bar{M}'}^{g_y,-} \pmod{2}, \end{aligned} \quad (\text{A10})$$

where

$$\gamma_L^+ = \gamma_L^{m_x,+} - \gamma_L^{g_y,+}, \quad (\text{A11})$$

and L labels the four lines at the interactions of mirror and glide invariant planes.

What we need to do next is just to show all terms except C_s on the right-hand side of Eq. (A10) add up to an even number. First, we can use Eq. (A8) to get

$$-2\gamma_{Z\bar{X}}^{g_y,+} - 2\gamma_{\bar{X}'Z}^{g_y,-} + 2\gamma_{\bar{Y}\bar{M}}^{g_y,+} - 2\gamma_{\bar{Y}\bar{M}'}^{g_y,-} \pmod{2} = -2\Phi_{V^{m_x,+,-},\bar{X}'Z} - 2\Phi_{V^{m_x,+,-},\bar{Y}\bar{M}'} \pmod{2} \quad (\text{A12})$$

where

$$\Phi_{U,L} = \frac{-i}{2\pi} \int_L d\mathbf{k} \cdot \text{Tr}[U^\dagger(\mathbf{k})\nabla_{\mathbf{k}}U(\mathbf{k})]. \quad (\text{A13})$$

Now, let us consider $\gamma_{ZZ'}^+$. With $g_y^2|\psi_{\mathbf{k}}\rangle = -e^{-ik_z}|\psi_{\mathbf{k}}\rangle$ and g_y being unitary, $V^{g_y}(0,0,k)$ must have the following form

$$V_{\alpha'\alpha}^{g_y,\beta',\beta}(0,0,k) = \begin{pmatrix} 0 & W_1(0,0,k) \\ -e^{-ik}W_1^\dagger(0,0,k) & 0 \end{pmatrix}_{\beta'\alpha',\beta\alpha}, \quad (\text{A14})$$

where $W_1(0,0,k)$ takes the indexes α' and α , is unitary, and satisfies $W_1(0,0,-\pi) = W_1(0,0,\pi)$. $V_{(0,0,k)}^{g_y}$ can be diagonalized by

$$U^{g_y,m_x}(0,0,k) = \frac{1}{\sqrt{2}} \begin{pmatrix} -ie^{ik/2}W_1(0,0,k) & ie^{ik/2}W_1(0,0,k) \\ 1 & 1 \end{pmatrix} \begin{pmatrix} W_2(0,0,k) & 0 \\ 0 & W_3(0,0,k) \end{pmatrix}, \quad (\text{A15})$$

where the boundary condition requires $W_2(0,0,\pm\pi) = W_3(0,0,\mp\pi)$ and both W_2 and W_3 matrices are unitary. As a result, $V^{m_x}(0,0,k)$ can be expressed by the W_2 and W_3 as

$$V^{m_x}(0,0,k) = -i \begin{pmatrix} 0 & W_2^\dagger(0,0,k)W_3(0,0,k) \\ W_3^\dagger(0,0,k)W_2(0,0,k) & 0 \end{pmatrix}. \quad (\text{A16})$$

With these relations, we can get

$$2\gamma_{Z'Z}^+ \pmod{2} = -\frac{N}{2} - 2\Phi_{W_2,Z'Z} \pmod{2} = -\frac{N}{4} + 2\phi_{V^{m_x,+,-},Z} \pmod{2}, \quad (\text{A17})$$

where $\phi_{U,\mathbf{k}} = \frac{(-i)}{2\pi} \log \det [U(\mathbf{k})]$. The same derivation can be applied to $\bar{Y}\bar{Y}$, $\bar{X}\bar{X}$, and $\bar{M}\bar{M}$, resulting in

$$\begin{aligned} & -2\gamma_{ZZ'}^+ - 2\gamma_{\bar{Y}\bar{Y}}^+ + 2\gamma_{\bar{X}\bar{X}}^+ + 2\gamma_{\bar{M}\bar{M}}^+ \pmod{2} = 2[\phi_{V^{m_x,+,-},Z} - \phi_{V^{m_x,+,-},\bar{Y}} - \phi_{V^{m_x,+,-},\bar{X}} + \phi_{V^{m_x,+,-},\bar{M}}] \pmod{2} \\ & = -2\Phi_{V^{m_x,+,-},Z\bar{X}} - 2\Phi_{V^{m_x,+,-},\bar{M}\bar{Y}} \pmod{2}. \end{aligned} \quad (\text{A18})$$

Combined the above equation, Eq. (A12), Eq. (A10), and $\Phi_{V^{m_x,+,-},\bar{X}'\bar{X}/\bar{M}'\bar{M}} \in \mathbb{Z}$, we arrive at Eq. (8) in the main text.

3. More details on the Tight-Binding Model for SG 26

In this section, we discuss the toy tight-binding (TB) model for SG 26 in more detail. There are two sublattice sites in one unit cell, $\boldsymbol{\tau}_1 = (0,0,0)$ and $\boldsymbol{\tau}_2 = (0,0,1/2)$. Then, in the real space, the bases of the Hamiltonian read $|\mathbf{R} + \boldsymbol{\tau}_i, s\rangle$, and the Fourier transformation of them gives

$$|\mathbf{k}, \boldsymbol{\tau}_i, s\rangle = \frac{1}{\sqrt{N_l}} \sum_{\mathbf{R}} e^{i(\mathbf{R}+\boldsymbol{\tau}_i)\cdot\mathbf{k}} |\mathbf{R} + \boldsymbol{\tau}_i, s\rangle, \quad (\text{A19})$$

where $s = \uparrow, \downarrow$ the spin index. The bases clearly satisfy $|\mathbf{k} + \mathbf{G}, \boldsymbol{\tau}_i, s\rangle = e^{i\mathbf{G}\cdot\boldsymbol{\tau}_i}|\mathbf{k}, \boldsymbol{\tau}_i, s\rangle$ for any reciprocal lattice vector \mathbf{G} . The glide and mirror symmetries are then represented as $g_y \doteq -ie^{-ik_z/2}\tau_x\sigma_y$ and $m_x \doteq -i\tau_0\sigma_x$, where τ 's and σ 's are Pauli matrices for sublattice and spin indexes.

Based on the symmetry representations, we consider the following Hamiltonian for the toy model

$$H = \sum_{\mathbf{k}, i, i', s, s'} |\mathbf{k}, \boldsymbol{\tau}_i, s\rangle [h(\mathbf{k})]_{ii', ss'} \langle \mathbf{k}, \boldsymbol{\tau}_{i'}, s' |, \quad (\text{A20})$$

$$h(\mathbf{k}) = d_1\tau_z\sigma_x + d_2\tau_y\sigma_0 + d_3\tau_x\sigma_0 + d_4\tau_z\sigma_z + d_5\tau_y\sigma_x, \quad (\text{A21})$$

where

$$\begin{aligned} d_1 &= m_0 - 3 + \cos(k_x) + \cos(k_y) + \cos(k_z), \\ d_2 &= \cos\left(\frac{k_z}{2}\right)\sin(k_y), \quad d_3 = \sin\left(\frac{k_z}{2}\right), \\ d_4 &= \sin(k_x), \quad d_5 = m_1 \cos\left(\frac{k_z}{2}\right)\cos(k_x), \end{aligned} \quad (\text{A22})$$

and the \mathbf{k} dependence of d_i 's is implied. The eigenvalues of Eq.(A21) can be analytically solved as $\pm\sqrt{d_1^2 + d_3^2 + (\sqrt{d_2^2 + d_4^2} \pm d_5)^2}$. We always consider the system at half filling.

From the eigenvalues of $h(\mathbf{k})$, we can derive the gapless condition as $d_1 = d_3 = 0$ and $|d_5| = \sqrt{d_2^2 + d_4^2}$, which, combined with the expressions of d_i 's, gives

$$\begin{aligned} \cos(k_x) &= \frac{-(m_0 - 2) \pm \sqrt{(m_0 - 2)^2 - (m_1^2 + 2)((2 - m_0)^2 - 2)}}{m_1^2 + 2}, \\ \cos(k_y) &= 2 - m_0 - \cos(k_x), \quad k_z = 0, \\ \cos(k_x) &\in \mathbb{R}, \quad |\cos(k_x)| \leq 1, \\ \cos(k_y) &\in \mathbb{R}, \quad |\cos(k_y)| \leq 1. \end{aligned} \quad (\text{A23})$$

Especially, the gapless points exist on $k_x = 0$ plane when

$$m_0 \in [0, 2], \quad m_1 = \pm\sqrt{m_0(2 - m_0)}; \quad (\text{A24})$$

the gapless points exist on $k_y = 0$ plane when

$$m_0 \in [0, 2], \quad m_1 = \pm\sqrt{\frac{1}{(1 - m_0)^2} - 1}. \quad (\text{A25})$$

With the above conditions, we plot Fig. 3(c) in the main text.

The Fermi arcs shown in Fig. 3(d) of in the main text are parts of the surface states on the (001) surface. The Fermi arcs are the intersection between the surface energy dispersion and the $E = 0$ plane. The surface energy dispersion turns out to be in a saddle-surface shape: the energy dispersion bends down along k_x -axis but bends up along k_y axis as shown in Fig. 6 (a) and (b), respectively.

Appendix B: Derivation of Eq. (9) in the main text

In this section, we derive Eq. (9) in the main text for systems without SOC in more detail. Recall that we assume that the system is gapped on $k_x = \pi$, $k_y = 0$, $k_y = \pi$, and $k_z = \pi$ planes, and has zero CN on $k_y = \pi$. All the four gapped planes are connected, and we can label the number of occupied band as N . This derivation has overlap with Ref. [55].

We first discuss ν_{g_y} . Since $C_{\mathcal{B}}$ is zero owing to the combination of inversion and glide symmetries $R_2 = g_y P$, we only need to consider the remaining parts that are only defined on the $k_y = 0, \pi$ planes. As discussed in the last section, the bands can have definite g_y eigenvalues, $\pm e^{-ik_z/2}$, on the $k_y = \Lambda$ plane, and the number of occupied bands with either eigenvalue should be equal to $N/2$, making N an even number. Then, we can choose the energy eigenstates

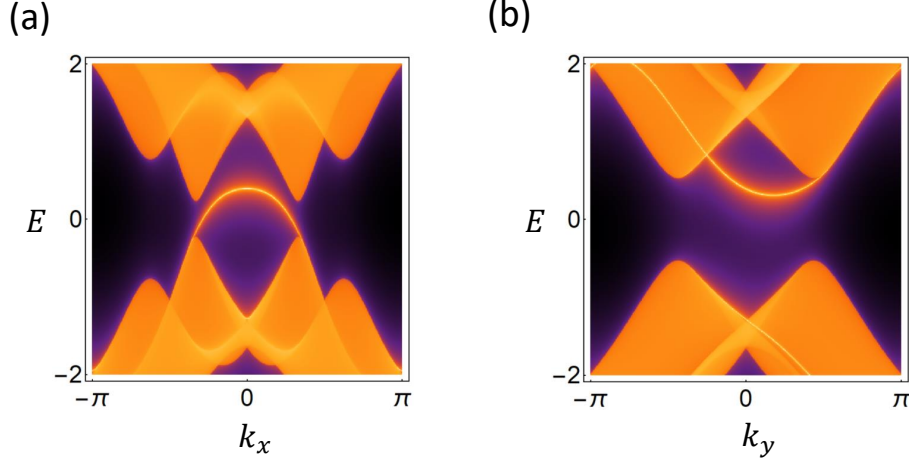


FIG 6. These two figures show the energy dispersion on (001) surface. (a) and (b) are for $k_y = 0$ and $k_x = 0$, respectively.

on $k_y = \Lambda$ as Eq.(A7) except that β now means the g_y eigenvalue $\beta e^{-ik_z/2}$ owing to the absence of SOC. From $Pg_y = e^{ip_z}g_yP$ and $P^2 = 1$, we have

$$P|\psi_{k_x, \Lambda, k_z}^{g_y, \beta, \alpha}\rangle = |\psi_{-k_x, \Lambda, -k_z}^{g_y, \beta, \alpha'}\rangle \left[V_P^{\beta, \beta}(k_x, \Lambda, k_z) \right]_{\alpha' \alpha} , \quad (\text{B1})$$

and the unitary $V_P^{\beta, \beta}(k_x, \Lambda, k_z)$ satisfies

$$V_P^{\beta, \beta}(k_x, \Lambda, k_z) V_P^{\beta, \beta}(-k_x, \Lambda, -k_z) = 1 . \quad (\text{B2})$$

The above relations give^{23,24}

$$C_{k_y=0}^{g_y, -} \bmod 2 = 2\gamma_{XX'}^{g_y, -} + 2\gamma_{X'X}^{g_y, -} \bmod 2 , \quad C_{k_y=\pi}^{g_y, -} \bmod 2 = 2\gamma_{MM'}^{g_y, -} + 2\gamma_{M'M}^{g_y, -} \bmod 2 , \quad (\text{B3})$$

resulting in

$$\nu_{g_y} = 2\gamma_{XX'}^{g_y, -} - 2\gamma_{MM'}^{g_y, -} \bmod 2 . \quad (\text{B4})$$

Combined with Eq.(B1), we have

$$\nu_{g_y} = 2(\phi_{V_P^{\beta, \beta}, X} - \phi_{V_P^{\beta, \beta}, \Gamma}) - 2(\phi_{V_P^{\beta, \beta}, M} - \phi_{V_P^{\beta, \beta}, Y}) \bmod 2 . \quad (\text{B5})$$

All four points, Γ , X , Y , and M , are on the $k_z = 0$ plane. On $k_z = 0$ plane, we have $[P, g_y] = 0$ meaning that the states at an inversion-invariant momentum K_0 on $k_z = 0$ plane can have definite P and g_y eigenvalues simultaneously, where P eigenvalue takes values ± 1 . We label the number of occupied states at K_0 with g_y eigenvalue $\beta e^{-ik_z/2}$ and P eigenvalue β' as $n_{K_0}^{g_y, \beta, P, \beta'}$, and then we have

$$\phi_{V_P^{\beta, \beta}, K_0} \bmod 1 = \frac{n_{K_0}^{g_y, -, P, -}}{2} \bmod 1 , \quad (\text{B6})$$

resulting in

$$\nu_{g_y} = \sum_{K_0} n_{K_0}^{g_y, -, P, -} \bmod 2 . \quad (\text{B7})$$

Now we simplify the expression of ν_P . Since $\{P, g_y\} = 0$ on $k_z = \pi$, the number of states with P eigenvalue $+1$ is equal to the number of states with P eigenvalue -1 at an inversion-invariant momentum on $k_z = \pi$ plane, which further equals to $N/2$. Combined with that N is even, we can first simply ν_P to

$$\nu_P = - \sum_{K_0} \frac{n_{K_0}^{P, -}}{2} \bmod 2 . \quad (\text{B8})$$

To simply the above equation, first note that $n_{K_0}^{P,-} = n_{K_0}^{g_y,+ ,P,-} + n_{K_0}^{g_y,- ,P,-}$ and $n_{K_0}^{g_y,+ ,P,-} + n_{K_0}^{g_y,+ ,P,+} = N/2$. Since the states at K_0 also have definite R_2 eigenvalues ± 1 , we have $n_{K_0}^{g_y,+ ,P,+} + n_{K_0}^{g_y,- ,P,-} = n_{K_0}^{R_2,+}$ with $n_{K_0}^{R_2,+}$ the number of occupied states with R_2 eigenvalue $+1$ at K_0 . As a result, we have

$$n_{K_0}^{P,-} = \frac{N}{2} - n_{K_0}^{R_2,+} + 2n_{K_0}^{g_y,- ,P,-} , \quad (\text{B9})$$

which further results in

$$\nu_P = \nu_{g_y} + \sum_{K_0} \frac{n_{K_0}^{R_2,+}}{2} \pmod{2}. \quad (\text{B10})$$

To obtain Eq. (9), the only thing left is to show that

$$\sum_{K_0} \frac{n_{K_0}^{R_2,+}}{2} - \frac{\Delta_{R_2}}{2} \quad (\text{B11})$$

is even, where $\Delta_{R_2} = n_{\Gamma}^{R_2,+} - n_Y^{R_2,+}$. First note that $n_X^{R_2,+} = n_M^{R_2,+}$ since $k_x = \pi$ is gapped, we have

$$\sum_{K_0} \frac{n_{K_0}^{R_2,+}}{2} - \frac{\Delta_{R_2}}{2} \pmod{2} = n_M^{R_2,+} + n_Y^{R_2,+} \pmod{2}. \quad (\text{B12})$$

Since the system has zero CN on $k_y = \pi$ plane, $n_M^{P,-} + n_Y^{P,-} + n_M^{P,-} + n_Y^{P,-}$ is even, and we have $n_M^{P,-} + n_Y^{P,-}$ is even owing to $n_M^{P,-} + n_Y^{P,-} = N$. As a result,

$$\begin{aligned} n_M^{R_2,+} + n_Y^{R_2,+} \pmod{2} &= n_M^{g_y,- ,P,-} + n_M^{g_y,+ ,P,+} + n_Y^{g_y,- ,P,-} + n_Y^{g_y,+ ,P,+} \pmod{2} \\ &= n_M^{g_y,- ,P,-} - n_M^{g_y,+ ,P,-} + n_Y^{g_y,- ,P,-} - n_Y^{g_y,+ ,P,-} \pmod{2} = n_M^{P,-} + n_Y^{P,-} \pmod{2} = 0 , \end{aligned} \quad (\text{B13})$$

from which we can get Eq. (9) of the main text.

At last, we would like to discuss a bit more about Eq. (9) of the main text. Since ν_{g_y} is always integer valued while ν_P is not, there are two cases that can make $\nu_P \neq \nu_{g_y}$: (i) $\nu_P=1/2$ or $3/2$ indicating that the system is gapless^{23,24}, and (ii) ν_P is an integer but different from ν_{g_y} . Δ_{R_2} is an odd number in case (i) and is twice an odd number in case (ii), both of which indicate the existence of the gapless points on the $\Gamma - Y$ axis given by the crossing between bands with different R_2 eigenvalues. When Δ_{R_2} is twice an even number and nonzero, the gapless points on the $\Gamma - Y$ axis still exist but they cannot be detected by the gapless criterion.
